

# Nanoscale

Accepted Manuscript



This is an *Accepted Manuscript*, which has been through the Royal Society of Chemistry peer review process and has been accepted for publication.

*Accepted Manuscripts* are published online shortly after acceptance, before technical editing, formatting and proof reading. Using this free service, authors can make their results available to the community, in citable form, before we publish the edited article. We will replace this *Accepted Manuscript* with the edited and formatted *Advance Article* as soon as it is available.

You can find more information about *Accepted Manuscripts* in the [Information for Authors](#).

Please note that technical editing may introduce minor changes to the text and/or graphics, which may alter content. The journal's standard [Terms & Conditions](#) and the [Ethical guidelines](#) still apply. In no event shall the Royal Society of Chemistry be held responsible for any errors or omissions in this *Accepted Manuscript* or any consequences arising from the use of any information it contains.

## Effect of Fullerenol Surface Chemistry on Nanoparticle Binding-induced Protein Misfolding

Slaven Radic<sup>1,\*</sup>, Praveen Nedumpully-Govindan<sup>1,2,\*</sup>, Ran Chen<sup>1</sup>, Emppu Salonen<sup>2</sup>, Jared M. Brown<sup>3</sup>, Pu Chun Ke<sup>1</sup>, and Feng Ding<sup>1</sup>

<sup>1</sup>Department of Physics and Astronomy, Clemson University, Clemson, SC 29634, USA

<sup>2</sup>Department of Applied Physics, Aalto University, FI-00076 Aalto, Finland

<sup>3</sup>Department of Pharmaceutical Sciences, Skaggs School of Pharmacy, University of Colorado Anschutz Medical Campus, Aurora, CO 80045, USA

\*These authors contributed equally

Address correspondence to: [fding@clemson.edu](mailto:fding@clemson.edu)

### Abstract

Fullerene and its derivatives with different surface chemistry have great potential in biomedical applications. Accordingly, it is important to delineate the impact of these carbon-based nanoparticles on protein structure, dynamics, and subsequently function. Here, we focused on hydroxylation — a common strategy for solubilizing and functionalizing fullerene — on protein-nanoparticle interactions using a model protein, ubiquitin. We applied a set of complementary computational modeling methods, including docking and molecular dynamics simulations with both explicit and implicit solvent, to illustrate the impact of hydroxylated fullerenes on the structure and dynamics of ubiquitin. We found that all derivatives bound to the model protein. Specifically, the more hydrophilic nanoparticles with a higher number of hydroxyl groups bound to the surface of the protein via hydrogen bonds, which stabilized the protein without inducing large conformational changes in the protein structure. In contrast, fullerene derivatives with a smaller number of hydroxyl groups buried their hydrophobic surface inside the protein, thereby causing protein denaturation. Overall, our results revealed a distinct role of surface chemistry on nanoparticle-protein binding and binding-induced protein misfolding.

**Keywords:** fullerene; fullerenol; nanoparticle; protein denaturation; nanotoxicity; nanomedicine;

Since their discovery, fullerene nanoparticles have attracted much attention due to their small sizes (~1 nm in diameter), caged structures, and distinct physicochemical properties. The ultrafine structures allow these nanoparticles to cross even the most difficult biological barriers, e.g. blood-brain barrier,<sup>1,2</sup> and reach different parts of the body, making them attractive drug and gene delivery vehicles.<sup>3,4</sup> Given their redox potentials as anti-oxidants<sup>5,6</sup> and relatively low toxicity,<sup>7</sup> fullerenes and their derivatives have also been investigated as novel drugs.<sup>4,8-11</sup> Specifically, functionalized fullerene derivatives have been found to inhibit the growth of sarcomas<sup>12</sup> and alleviate allergic responses.<sup>13</sup> Like many other types of nanoparticles, fullerene derivatives can bind to a wide range of proteins upon entering a biological system. For instance, it was found that fullerenes can bind to HIV protease,<sup>8</sup> influenza viruses,<sup>10</sup> serum albumin<sup>14,15</sup>

and fullerene specific antibodies.<sup>16</sup> In light of the fact that increasing production and potential biomedical applications will eventually lead to human exposure to these carbon-based nanoparticles, it is essential to delineate the effect of fullerene-binding on the structure, dynamics and subsequent functioning of proteins, the building blocks of cellular life.

A major limitation for the use of pristine fullerene C<sub>60</sub> has been its low solubility in water, and the need for special treatments like sonication, encapsulation in special carriers or use of co-solvents.<sup>4</sup> Alternatively, these hydrophobic nanoparticles can be functionalized with polar groups to better enable their designed biological and biomedical applications. One of the common functionalization strategies is hydroxylation, where polar hydroxyl (-OH) groups are chemically attached to the surface of fullerene nanoparticles to render soluble fullerenols.<sup>4,17</sup> Depending on the particular chemical procedures used to hydroxylate the fullerene, the number of OH groups on the hydroxylated fullerene (i.e., fullereneol C<sub>60</sub>(OH)<sub>n</sub>) may vary, assuming values of n=4, 6, 8, 20, 24, and 36,<sup>18-21</sup> for example. As one would expect, the solubility of fullereneol particles increases as the number of hydroxyl group is increased.<sup>22</sup> However, the effect of variations in nanoparticle surface chemistry on protein-fullereneol binding, including both structure and dynamics of protein-nanoparticle complex on the molecular and atomic levels, is largely unknown.

Various computational studies have been conducted in order to uncover the molecular mechanisms of the interactions between proteins and various fullerene derivatives. Using molecular dynamics (MD) simulations, hydroxylated fullerenols C<sub>60</sub>(OH)<sub>20</sub> were bound to tubulin<sup>23</sup> and *taq* DNA polymerase<sup>24</sup> via the formation of hydrogen bonds. Fullerenes were also investigated *in silico* as a potential potassium channel blocker.<sup>25</sup> Through molecular modeling, fullerenes conjugated with small ligands were exploited as potential drugs to competitively bind the active sites of HIV-1 protease<sup>8</sup> and H5N3 influenza virus endonuclease.<sup>10</sup> Most of these previous studies, however, focused on either pristine fullerenes or highly hydroxylated fullerenols. Recently, molecular docking has been applied to investigate the influences of size and extent of hydroxylation of fullerenols on their interactions with a variety of proteins, including RNA reverse transcriptase, RNase A, HIV-1 protease and tubulin.<sup>26</sup> It was found that the driving force of protein-fullereneol interaction was  $\pi$ -stacking and the increased number of hydroxyl groups resulted in a decreased binding affinity. However, since molecular docking studies assumed the protein conformation static or with only minor changes, variations in protein structure and dynamics upon nanoparticle binding as observed in many experiments<sup>23,27,28</sup> cannot be obtained.

Here, we applied a set of computational methods, including both docking and MD simulations, to systematically study the effect of fullereneol surface chemistry on its interaction with proteins, with the focus on changes in protein structure and dynamics. We used ubiquitin as the model protein since it is ubiquitously expressed in all eukaryotic cells<sup>29</sup> regulating protein distribution and recycling,<sup>30</sup> thus rendering our study both biologically and ecologically relevant. Specifically, we performed atomistic MD simulations with both explicit and implicit solvents. For the implicit solvent simulations, we used discrete molecular dynamics (DMD) simulations, a rapid conformational dynamics sampling algorithm<sup>31</sup> for biomolecules and molecular complexes. Compared to all-atom MD simulations with explicit solvent, DMD simulations with implicit solvents are able to reach longer time scales, which allowed direct observation of protein folding

*ab initio*<sup>32,33</sup> and the observation of nanoparticle-protein corona formation.<sup>34,35</sup> For highly hydroxylated fullerenols, both our conventional MD and DMD simulations suggested that the nanoparticles bound to the surface of ubiquitin via hydrogen bonds and the protein maintained its native structure. As a proof of the concept and in consideration of technical difficulty in accurately controlling the number of hydroxyl groups on the fullereneol, experimental measurements of protein-fullereneol binding were carried out only for a highly hydroxylated fullereneol, C<sub>60</sub>(OH)<sub>20</sub>. We find that the binding sites of C<sub>60</sub>(OH)<sub>20</sub> derived from both docking and MD simulations are consistent with our fluorescence and isothermal titration calorimetry (ITC) measurements. As the number of hydroxyl groups decreased and the nanoparticles became subsequently more hydrophobic, both DMD and MD simulations revealed that the nanoparticles bound the protein via hydrophobic interaction and  $\pi$ -stacking. Only in DMD simulations, we were able to observe large-scale protein conformational dynamics that takes place on longer time scales, allowing the hydrophobic nanoparticle to partition into the protein core and subsequently disrupt the native protein structure. Overall, our results indicate that fullerenols with limited hydroxylation can induce protein misfolding, which could potentially trigger protein aggregation and adverse biological responses.<sup>36,37</sup>

## Results and Discussions

Due to its high solubility and commercial availability, fullereneol with ~20 hydroxyl groups C<sub>60</sub>(OH)<sub>20</sub> (buckyusa.com) is one of the most well-studied fullerene derivatives in both experiments<sup>23,38–40</sup> and simulations.<sup>23,24,38,41–43</sup> Therefore, we first focused on the binding of C<sub>60</sub> and C<sub>60</sub>(OH)<sub>20</sub> to ubiquitin using various computational methods, including molecular docking, MD (explicit solvent) and DMD (implicit solvent) simulations. The simulation results of C<sub>60</sub>(OH)<sub>20</sub> were compared to experimental characterizations by fluorescence quenching, ITC, and circular dichroism (CD) spectroscopy. Experiments with pristine and low hydroxylated fullerenes were not carried out due to their poor solubility.

**Fullerene C<sub>60</sub> and fullereneol C<sub>60</sub>(OH)<sub>20</sub> binding with ubiquitin.** First, docking simulations were performed to identify the potential binding sites of C<sub>60</sub> and C<sub>60</sub>(OH)<sub>20</sub> nanoparticles on ubiquitin (Methods). The fullereneol nanoparticles showed two preferred binding sites on ubiquitin (see Fig. 1A). In 57% of docking simulations, C<sub>60</sub>(OH)<sub>20</sub> bound to the protein surface region near residues 59–63, while in another 34% of simulations binding took place near the protein C-terminal (see Fig. S1 for a detailed view of the binding sites). The binding scores for these two sites are 8.2 and 8.1 kcal/mol, respectively. On the other hand, pristine fullerene showed only one predominant binding site that was similar to the first binding site of fullereneol, near residues 60–63 (Fig. 1B). The nanoparticle bound to this site in 90% simulations, with a binding score of 7.1 kcal/mol.

Next, we performed both MD and DMD simulations of nanoparticle-ubiquitin binding (Methods). We started the simulations by placing 13 C<sub>60</sub> or C<sub>60</sub>(OH)<sub>20</sub> nanoparticles randomly around the protein. High nanoparticle-protein stoichiometry (13:1) was set up in order to observe multiple protein-nanoparticle binding events in one simulation. In both DMD and MD simulations, the hydrophilic C<sub>60</sub>(OH)<sub>20</sub> nanoparticles bound to the protein surface at various locations via diffusion. Once bound, the particles started to diffuse on the protein surface and

eventually formed clusters near the preferred binding sites. The final structures from MD (Fig. 1C) and DMD (Fig. 1E) simulations are highly similar, where the protein maintained its native-like structure while the nanoparticles form clusters near two similar binding sites. Interestingly, the two binding sites observed in MD and DMD simulations agree with those obtained from docking simulations. The binding in the proximity of TYR59 residue is also consistent with our fluorescence quenching experiment. Ubiquitin possesses only one tyrosine (TYR59), whose fluorescence intensity was measured for four different concentrations of  $C_{60}(OH)_{20}$  at a given ubiquitin concentration. A linear static quenching of fluorescence intensity was observed with increasing  $C_{60}(OH)_{20}$  concentration (Fig. S2). This observation indicates that  $C_{60}(OH)_{20}$  molecules bound the protein specifically in the proximity of TYR59. The binding was further characterized by ITC measurement, which showed that an average of 1.3 fullereneol molecules bound to the protein (Fig. S3). This observation can be explained by the fullereneol preferential binding to two distinct sites of ubiquitin (near TYR59 and C-terminal). Different binding affinities of these two sites might result in the fullereneol:protein stoichiometry less than 2. Both the fluorescence quenching and ITC experiments indicated that the binding affinity between  $C_{60}(OH)_{20}$  and ubiquitin is 10–100  $\mu$ M. The ITC derived stoichiometry is consistent with the simulation result of two binding sites per protein. Therefore, both our simulations and experiments are in agreement in terms of ubiquitin- $C_{60}(OH)_{20}$  binding, highlighting the predictive power of computational modeling for addressing nanoparticle-protein interactions.

In the fullerene-protein binding simulations, we found that the final protein structures from MD (Fig. 1E) and DMD (Fig. 1F) simulations were drastically different. In the DMD simulations, specifically, the hydrophobic fullerene nanoparticles eventually moved from the surface into the hydrophobic core of the protein. As a result, the protein was partially denatured with only a few native secondary structural elements remaining intact. Similar large protein conformational changes induced by binding of various types of hydrophobic carbon-based nanoparticles have been observed in both experiments<sup>44</sup> and simulations.<sup>45</sup> For example, serum proteins were found to undergo large conformational changes in the presence of multi-walled carbon nanotubes,<sup>44</sup> while MD simulations showed that a single-walled carbon nanotube was able to partition into the core of a WW-domain protein to disrupt its native structure.<sup>45</sup> However, such large conformational changes were not observed in our accompanying MD simulations of fullerene-ubiquitin binding, where nanoparticles remained on the protein surface with similar binding sites as that for  $C_{60}(OH)_{20}$  and the protein maintained its native-like structure. We hypothesize that the differential structures observed in the MD and DMD simulations of fullerene-ubiquitin binding are the result of the different time scales that can be reached by implicit and explicit solvent within similar simulation times. Without friction due to solvent molecules, protein dynamics is known to be faster in implicit solvent simulations.<sup>46</sup> The key question here is given the same time scales in DMD simulations why  $C_{60}$  was able to denature the protein while  $C_{60}(OH)_{20}$  was not. Next, we examined protein conformational dynamics in the presence of different nanoparticles using DMD simulations.

**Differential protein conformational dynamics induced by  $C_{60}$  and  $C_{60}(OH)_{20}$ .** To avoid the complexity of nanoparticle-nanoparticle and nanoparticle cluster-protein interactions, we performed DMD simulations of a single nanoparticle,  $C_{60}$  and  $C_{60}(OH)_{20}$ , interacting with a single protein ubiquitin. We monitored the root-mean-square deviations (RMSD) of protein conformation with respect to its native structure, the center-of-mass distance between the protein

and the nanoparticle ( $d_{CM}$ ), and the number of protein residues ( $N_C$ ) in contact with the nanoparticle (typical simulation trajectories exemplified in Fig. 2). A residue was considered in contact with the nanoparticle if any of its heavy atoms were within 5 Å of the nanoparticle heavy atoms. Upon binding  $C_{60}(OH)_{20}$ , the RMSD value of the protein fluctuated around 2–3 Å with transient, large fluctuations occasionally approaching 4 Å (Fig. 2B) as observed in DMD simulations of ubiquitin alone without nanoparticle (Fig. S4). The contact number between protein and nanoparticle remained within 15 Å while the nanoparticle stayed on the protein surface with  $d_{CM} > 15$  Å (e.g., the snapshot structures along the trajectory in Fig. 2B).

In the case of  $C_{60}$ , the initial fluctuations of RMSD, contact numbers, and intermolecular distance  $d_{CM}$  upon nanoparticle binding were similar to those of  $C_{60}(OH)_{20}$  binding (Figs. 2A,B). After some large conformational fluctuations with RMSD around 2–3 Å ( $3.5 \times 10^5 - 5 \times 10^5$  DMD time unit, t.u.), the contact number  $N_C$  increased to  $> 20$  while the intermolecular distance  $d_{CM}$  reduced to  $\sim 5$  Å. Eventually, the RMSD of the protein increased above 4 Å. The snapshot structure (inserts of Fig. 2A) indicated that the protein partially unfolded as the nanoparticle partitioned into the protein.

Taken together, since larger conformational changes often require higher energy changes and thus have lower probabilities for occurrence, the longer effective time scales in the DMD simulations allowed the observation of ubiquitin conformational dynamics with larger RMSD values (Fig. 2 and Fig. S4) compared to the MD simulations with explicit solvent (Fig. S5). The observed  $C_{60}$ -ubiquitin structures in MD simulations (Fig. 1D) were consistent with the initial phases of  $C_{60}$  binding with ubiquitin, where nanoparticles remained on the protein surface without denaturing the protein (Fig. 2). With large conformational changes populated along the DMD simulation trajectory, the protein partially exposed its hydrophobic core and the hydrophobic  $C_{60}$  was able to plug into the protein core to cause denaturation. On the other hand, the hydrophilic  $C_{60}(OH)_{20}$  stayed on the protein surface as the protein folded back into its native state, results in transient large conformational fluctuations as observed also in DMD simulations of ubiquitin without any nanoparticles (Fig. S4). Therefore, the major reason for the differential protein dynamics upon binding to the nanoparticles is the difference in the nanoparticle surface chemistry — the number of hydroxyl groups. Next, we performed DMD simulations of protein binding with nanoparticles of different extent of hydroxylation.

**Ubiquitin-fullerenol binding with different extent of hydroxylation.** We investigated the interactions between ubiquitin and nanoparticles with intermediate hydroxylation, including 4, 8, 12 and 16 hydroxyl groups and thus having intermediate surface hydrophobicity as well as various degrees of hydrogen bond donors and acceptors (Fig. 3A). For each fullerenol derivative, we performed DMD simulations with a single nanoparticle and a single protein. To avoid potential bias of initial condition and to increase sampling statistics, we performed 20 independent simulations with different initial intermolecular positions and orientations (Methods). Based on the independent DMD simulations, we calculated distributions of the intermolecular distance  $d_{CM}$  (Fig. 3B), the number of residue contacts  $N_C$  (Fig. 3C), and the protein RMSD (Fig. 3D). We found that as the number of surface hydroxyl groups decreased the fullerenol exhibited an increased probability to penetrate into the protein core (with low  $d_{CM} < 10$  Å and large number of residue contacts  $N_C > 20$ ) and consequently denatured the protein (with RMSD  $> 4$  Å). Interestingly, we found that these nanoparticles can be approximately divided

into two categories based on their binding behaviors, i.e., the more hydrophobic  $C_{60}$ ,  $C_{60}(OH)_4$ , and  $C_{60}(OH)_8$ , and the more hydrophilic  $C_{60}(OH)_{12}$ ,  $C_{60}(OH)_{16}$ , and  $C_{60}(OH)_{20}$ . The more hydrophobic fullerlenols ( $C_{60}(OH)_4$  and  $C_{60}(OH)_8$ ) behaved like the pristine fullerene  $C_{60}$ , while  $C_{60}(OH)_{12}$  and  $C_{60}(OH)_{16}$  were similar to  $C_{60}(OH)_{20}$  (Figs. 3B-D). Due to smaller number of surface hydroxyls, the hydrophobic fullerlenols have large hydrophobic patches on the surface, which can be buried inside the protein and thus disrupt the protein native structure. As the number of hydroxyl groups increases, the available hydrophobic patches and their sizes decrease, which allow the nanoparticles to stay on the protein surface upon protein binding.

In order to quantify the detailed binding between fullerlenol and protein residues, we computed the average contact frequency between each residue and the corresponding nanoparticle (Fig. 4). We colored the residues in the protein structure according to their binding frequencies (Fig. 4B). Compared to the more hydrophilic fullerlenols, i.e.,  $C_{60}(OH)_n$  with  $n \geq 12$ , the binding of the more hydrophobic ( $n < 12$ ) nanoparticles with the protein appeared mostly non-specific, including significant probabilities to interact with the buried residues. As the number of hydroxyl groups increased, the binding of hydrophilic fullerlenols with the protein became more specific. For instance, the binding sites of fullerlenol  $C_{60}(OH)_{20}$  include the region near TYR59 and C-terminal (Fig. 4B). The C-terminal binding has a weaker probability (yellow color) compared to the binding near TYR59 (red color), consistent with the estimated binding probabilities from docking simulations.

Even though solubility increases as more hydroxyl groups are added to the nanoparticle surface,<sup>22</sup> our simulation study suggests that, compared to pristine fullerene  $C_{60}$ , fullerlenol  $C_{60}(OH)_8$  was still able to denature the bound proteins. Possibly due to the small size of the fullerlenol nanoparticle, the extent of protein conformational change upon binding a single nanoparticle was relatively small as the increase of RMSD was relatively small (Figs. 2,3). Next, we examined the effect of multiple fullerlenol binding on ubiquitin secondary or tertiary structures.

**Protein structural changes upon fullerlenol binding.** We performed DMD simulations with a ubiquitin protein interacting with multiple fullerlenols of  $C_{60}(OH)_n$ , where  $n=0, 8, 20$ . Multiple independent simulations with different initial conditions were performed to enhance the sampling statistics. Averaged over the independent simulations, we computed the protein RMSD as the function of simulation time (Fig. 5A). Fullerene  $C_{60}$  had the greatest effect in terms of protein denaturation, with the highest RMSD of  $\sim 8 \text{ \AA}$  at the end of the DMD simulations. The protein core was loaded with multiple nanoparticles (Figs. 1,5). As expected, fullerlenol  $C_{60}(OH)_8$  was also able to denature the protein, with  $\text{RMSD} > 4.5 \text{ \AA}$ ; however, these nanoparticles could not fully penetrate the protein and were partially buried into the protein (Fig. 5A) to compromise the structure of the protein. Interestingly, the  $C_{60}(OH)_{20}$ -bound ubiquitin exhibited a smaller RMSD compared to the reference simulations where the nanoparticle was absent. The decreased RMSD in the presence of  $C_{60}(OH)_{20}$  is likely due to the fact that a high number of surface hydroxyl groups on the nanoparticle surface was able to establish multiple hydrogen bonds with the protein side chains, thereby reducing their thermal fluctuations.

To estimate the changes in protein secondary structures upon nanoparticle binding, we also calculated the average secondary structure contents of the ubiquitin using a method

proposed by Srinivasan and Rose<sup>47</sup> (Fig. 5B). The average was taken over multiple independent simulations. Compared to the reference simulations of ubiquitin alone, binding of fullerene and various fullerenols consistently reduced the content of  $\alpha$ -helices and turns, and increased the amount of random coils. The changes in  $\beta$  strands are relatively small without obvious trends. Among the modeled nanoparticles, fullerene  $C_{60}$  had the strongest effects in terms of affecting protein secondary structures. Experimentally, due to solubility and availability issues, we only performed CD measurements of ubiquitin alone and ubiquitin incubated with  $C_{60}(OH)_{20}$  (Methods; Fig. S6 and Fig. 5C). The experimentally measured changes in secondary structure contents were qualitatively consistent with the predicted changes derived from DMD simulations. Although there are differences in the absolute values of secondary structure contents between experiments and simulations, the changes upon fullerenol bonding are in accord with each other, including slight decreases in alpha helices, and increases in  $\beta$  sheets and random coil content (Figs. 5B,C).

## Conclusion

We studied the binding of ubiquitin with fullerene and its fullerenol derivatives,  $C_{60}(OH)_n$  with various number of hydroxyls,  $n$ . In the case of  $C_{60}(OH)_{20}$  for which experiments were performed, agreement between experimental measures (including ITC, fluorescence quenching, and CD) and various computational methods (docking, MD with explicit solvent, and DMD with implicit solvent) underscore the predictive power of computational modeling for nanoparticle-protein interaction. Most importantly, the ability of DMD simulations to sample longer time scales than traditional MD simulations with explicit solvent allowed the observation of protein denaturation with hydrophobic fullerene  $C_{60}$ . Due to the low solubility of pristine  $C_{60}$ , we could not perform the corresponding experimental measurements to verify the nanoparticle binding-induced misfolding of ubiquitin. On the other hand, the denaturation of proteins by hydrophobic carbon-based nanoparticles other than  $C_{60}$  has already been observed experimentally.<sup>44,48-50</sup> Therefore, our study has shown that DMD simulations can be used as an efficient tool for unraveling the complex phenomena at the nano-bio interface, such as delineating the structure and dynamics of nanoparticle-protein corona<sup>51</sup> in order to better understand nanotoxicity and thereby enable improved applications of nanomedicine.

The surface chemistry of nanoparticles is an important determinant of their interactions with proteins in addition to the nanoparticle size and shape.<sup>51</sup> In this work, we studied the effect of different extent of hydroxylation in computation simulations, where the surface hydroxyl groups can serve as both donor and acceptor for hydrogen bonding. Our results suggested that different extent of hydroxylation had significant effects on  $C_{60}(OH)_n$ -protein interactions. Specifically, fullerenols with  $n \leq 8$  were able to denature the protein since their relatively small number of hydroxyls allowed more hydrophobic patches on the nanoparticle surface (Fig. 3A) and significant interactions with the protein hydrophobic core to disturb its tertiary structure. Hydrophilic nanoparticles, in contrast, remained bound on the protein surface without inducing major structural changes. In fact, hydrophilic particles, especially  $C_{60}(OH)_{20}$ , could form multiple hydrogen bonds with protein surface residues to reduce structural fluctuations (Fig. 5A). Taken together, our study revealed a distinctive role of surface hydroxylation in term of nanoparticle-binding induced protein misfolding. With the advancement of computational

modeling of the nano-bio interface and improvement of the predictive power, it might be possible to accurately adjust the nanoparticle surface chemistry in order to reduce the potential adverse effects such as nanoparticle-binding induced protein misfolding and concomitantly increase the nanoparticle biocompatibility.

## Methods

**Docking.**  $C_{60}$  and  $C_{60}(\text{OH})_{20}$  were docked on to human erythrocyte ubiquitin structure obtained from the protein data bank (PDB ID: 1UBQ<sup>52</sup>). Three of 76 residues of this structure are different from the *A. thaliana* ubiquitin, which was used in experiments. Docking simulations were performed using AutoDock 4.2 docking software<sup>53</sup> with its default force field. Fifty docking simulations, each with 10 trials, were carried out keeping both protein and nanoparticles rigid. A Lamarckian genetic algorithm<sup>53</sup> with  $2.5 \times 10^7$  evaluations was used. The resulting docked poses were clustered based on their mutual root-mean-square deviation values, using a cutoff of 0.8 nm. Here, the larger than usual cutoff value of 0.2 nm was used because the nanoparticle was able to bind the same site by rotating around its center of mass.

**Molecular Dynamics (MD).** The MD simulations were carried out using GROMACS simulation package version 4.5.4<sup>54</sup> with OPLSAA force field<sup>55,56</sup> for protein and a compatible parameter set for nanoparticles as described elsewhere<sup>24</sup>. The protein-nanoparticle complex was placed in a simulation box whose edges were at least 0.9 nm away from the solute. The box was then filled with TIP4P<sup>57</sup> water molecules.  $\text{Na}^+$  and  $\text{Cl}^-$  ions were added so that the simulation box had an ion concentration of 100 mM. The system was energy minimized between each of these steps using steepest descent algorithm. First, the simulation system was equilibrated with a 50 ps long NVT simulation, which was followed by a 100 ps long NPT simulation. During these equilibrium runs, the temperature and pressure of the system were coupled using the Bussi-Donadio-Parrinello velocity rescale algorithm<sup>58</sup> (298 K,  $\tau_T = 1$  ps) and Berendsen weak coupling algorithm<sup>59</sup> (1 bar,  $\tau_p = 4$  ps, only for NPT simulation), respectively. For production runs, the Bussi-Donadio-Parrinello velocity rescaling algorithm and Parrinello-Rahman algorithm<sup>60</sup> were used for temperature (298 K,  $\tau_T = 1$  ps) and pressure coupling (1 bar,  $\tau_p = 4$  ps), respectively. Six independent copies of each simulation were carried out, each lasting 100 ns. The simulation time step was set at 2 fs with all bonds constrained using the LINCS algorithm.<sup>61</sup> The electrostatic interactions were treated with smooth PME method,<sup>62,63</sup> with a cut-off of 0.9 nm. For Lennard-Jones interactions a cut-off of 1.4 nm was used without any switch or shift functions.

**Discrete Molecular Dynamics (DMD).** Detailed descriptions for DMD algorithm can be found elsewhere.<sup>32,33</sup> Briefly, inter-atomic interactions in DMD were modeled by square-well potential functions. Neighboring interactions (such as bonds, bond angles, and dihedrals) were modeled by infinitely deep square-well potentials. During a simulation, an atom's velocity remained constant until a potential step was encountered, upon which time it changed instantaneously according to the conservations of energy, momentum, and angular momentum. Simulations proceeded as a series of such collisions, with a rapid sorting algorithm used at each step to determine the subsequent collision.

In our DMD simulations, fullerene derivatives with 0, 4, 8, 12, 16 hydroxyl groups were

prepared by randomly removing –OH groups from fullerene, whose structure was taken from a previous C<sub>60</sub>(OH)<sub>20</sub> model.<sup>23,49</sup> The system was modeled and visualized using PyMOL.<sup>64</sup> Single nanoparticle simulations were carried out at room temperature 300 K. Dimensions of the simulation box were set at 75 Å in all three dimensions and periodic boundary conditions were imposed. Prior to simulation, ubiquitin and the nanoparticle were positioned away from each other. Initially, system was equilibrated for 5 ns and followed by 50 ns production simulations. Twenty independent simulations with different initial conditions, including relative intermolecular distance and orientation as well as velocities, were performed in order to reduce the sampling bias of initial conditions and to increase sampling statistics. During the simulation we monitored protein RMSD. For comparison, multiple independent simulations of ubiquitin alone without nanoparticles were performed without any nanoparticle.

For the study of ubiquitin binding with multiple nanoparticles, 13 nanoparticles and one protein were initially positioned away from each other in a cubic simulation box of 100 Å. We chose to simulate three representative cases: insoluble fullerene C<sub>60</sub>, partially hydrophobic C<sub>60</sub>(OH)<sub>8</sub> and hydrophilic fullerene C<sub>60</sub>(OH)<sub>20</sub>. For each case, 10 independent DMD simulations were performed and each simulation followed the same protocol as the single nanoparticle binding simulations.

*Fullerenol Preparation.* A stock of fullerenols (BuckyUSA) 1 mg/ml dispersed in Milli-Q was firstly sonicated and then the new 10x diluted filtered stock was made for the measurements. Filtration was done with Anotop filters (0.1 µm, Whatman).

*Fluorescence measurements.* Further study of the ubiquitin fullerene interaction was done by fluorescence quenching study of ubiquitin (*A. thaliana*) tyrosine (Y) residue (amino acid sequence: MQIFVKTLTGKTITLEVESSDTIDNVKAKIQDKEGIPPDQQLIFAGKQLEDGRT LADYN IQKESTLHLV LRLRGG) by adding fullerenols into solution. The experiment was performed on a Varian Eclipse fluorometer. Concentrations of added fullerene in solution were 9.43 mM, 15.7 mM, 23.6 mM, and 47.2 mM, while the ubiquitin concentration was held constant at 10 mM. The mixtures were incubated for 2 h before the measurement. The excitation wavelength was 220 nm and the observed emission was 303 nm, which is the emission wavelength characteristic for tyrosine residue. We fitted data with the Stern-Volmer equation:<sup>65</sup>

$$\frac{I_0}{I} = 1 + K_b C_{Fullerenol}$$

where  $I_0$  is emission intensity of the ubiquitin without added fullerene, and  $I$  is the emission intensity of ubiquitin when fullerene with a concentration of  $C_{Fullerenol}$  is added to the protein.

To account for apparent quenching, we corrected our intensities considering our cell geometric and absorption characteristics. The correction is described by Parker equation.<sup>66</sup>

$$\frac{I_{corrected}}{I_{observed}} = \frac{2.3dA_{ex}}{1 - 10^{-dA_{ex}}} \times \frac{2.3sA_{ex}}{1 - 10^{-sA_{ex}}} \times 10^{gA_{em}}$$

Where  $I_{corrected}$  and  $I_{observed}$  are the corrected and observed intensities,  $A_{ex}$  and  $A_{em}$  are absorbance per centimeter at the excitation and emission wavelengths, and parameters  $s$ ,  $g$  and  $d$  depend on the geometry of the measurement.

*Isothermal titration calorimetry (ITC).* The thermal dynamics of the binding between fullereneol and ubiquitin was investigated using an isothermal titration calorimeter (ITC, TAM III, TA Instruments). 1.88 mM of fullereneol solution (in Milli-Q water) was placed in the glass syringe, and then was titrated into the ampoule containing 0.1 mM ubiquitin solution (in Milli-Q water) at the rate of 9.975  $\mu$ L per injection. The time interval between two consecutive injections was set to 15 min, and total 25 injections were performed. The raw data was pre-processed using TAM Assistant, and imported into NanoAnalyze, then fitted using the built-in Independent Model to render the thermal dynamics of the binding, which yields  $n=3.083$ ,  $K_a=6.324 \times 10^4 \text{ M}^{-1}$ ,  $\Delta H=16.83 \text{ kJ/mol}$ ,  $K_d=1.581 \times 10^{-5} \text{ M}$ , and  $\Delta S=148.3 \text{ J/mol.K}$ .

### Acknowledgements

The work was supported in part by the NSF Grant CBET-1232724 (to P.C.K.), an NIEHS grant R01 ES019311 02S1 (to J.M.B. and P.C.K.), Academy of Finland project no. 127091 (to E.S.) and the startup funds from Clemson University (to F.D.).

**Supporting information available:** Electronic supplementary information (ESI) is available for Fluorescence spectra, ITC, CD spectra and other data as described in the text.

### References

- (1) Yamago, S.; Tokuyama, H.; Nakamura, E.; Kikuchi, K.; Kananishi, S.; Sueki, K.; Nakahara, H.; Enomoto, S.; Ambe, F. In Vivo Biological Behavior of a Water-Miscible Fullerene:  $^{14}\text{C}$  Labeling, Absorption, Distribution, Excretion and Acute Toxicity. *Chem. Biol.* **1995**, *2*, 385–389.
- (2) Oberdorster, E. Manufactured Nanomaterials (Fullerenes, C60) Induce Oxidative Stress in the Brain of Juvenile Largemouth Bass. *Environ. Health Perspect.* **2004**, *112*, 1058–1062.
- (3) Lin, C.-M. C60 Fullerene Derivatized Nanoparticles and Their Application to Therapeutics. *Recent Pat. Nanotechnol.* **2012**, *6*, 105–113.
- (4) Da Ros, T.; Prato, M. Medicinal Chemistry with Fullerenes and Fullerene Derivatives. *Chem Commun* **1999**, 663–669.
- (5) Wang, I. C.; Tai, L. A.; Lee, D. D.; Kanakamma, P. P.; Shen, C. K.-F.; Luh, T.-Y.; Cheng, C. H.; Hwang, K. C. C60 and Water-Soluble Fullerene Derivatives as Antioxidants Against Radical-Initiated Lipid Peroxidation. *J. Med. Chem.* **1999**, *42*, 4614–4620.
- (6) Gharbi, N.; Pressac, M.; Hadchouel, M.; Szwarc, H.; Wilson, S. R.; Moussa, F. [60]Fullerene Is a Powerful Antioxidant in Vivo with No Acute or Subacute Toxicity. *Nano Lett.* **2005**, *5*, 2578–2585.
- (7) Kolosnjaj, J.; Szwarc, H.; Moussa, F. Toxicity Studies of Fullerenes and Derivatives. In *Bio-Applications of Nanoparticles*; Chan, W. C. W., Ed.; Advances in Experimental Medicine and Biology; Springer New York, 2007; pp. 168–180.
- (8) Tzoupis, H.; Leonis, G.; Durdagi, S.; Mouchlis, V.; Mavromoustakos, T.; Papadopoulos, M. G. Binding of Novel Fullerene Inhibitors to HIV-1 Protease: Insight through Molecular

- Dynamics and Molecular Mechanics Poisson–Boltzmann Surface Area Calculations. *J. Comput. Aided Mol. Des.* **2011**, *25*, 959–976.
- (9) Friedman, S. H.; DeCamp, D. L.; Sijbesma, R. P.; Srdanov, G.; Wudl, F.; Kenyon, G. L. Inhibition of the HIV-1 Protease by Fullerene Derivatives: Model Building Studies and Experimental Verification. *J. Am. Chem. Soc.* **1993**, *115*, 6506–6509.
- (10) Shoji, M.; Takahashi, E.; Hatakeyama, D.; Iwai, Y.; Morita, Y.; Shirayama, R.; Echigo, N.; Kido, H.; Nakamura, S.; Mashino, T.; *et al.* Anti-Influenza Activity of c60 Fullerene Derivatives. *PloS One* **2013**, *8*, e66337.
- (11) Yin, X.; Zhao, L.; Kang, S.; Pan, J.; Song, Y.; Zhang, M.; Xing, G.; Wang, F.; Li, J.; Zhou, R.; *et al.* Impacts of Fullerene Derivatives on Regulating the Structure and Assembly of Collagen Molecules. *Nanoscale* **2013**, *5*, 7341–7348.
- (12) Yumita, N.; Iwase, Y.; Imaizumi, T.; Sakurazawa, A.; Kaya, Y.; Nishi, K.; Ikeda, T.; Umemura, S.-I.; Chen, F.-S.; Momose, Y. Sonodynamically-Induced Anticancer Effects by Functionalized Fullerenes. *Anticancer Res.* **2013**, *33*, 3145–3151.
- (13) Ryan, J. J.; Bateman, H. R.; Stover, A.; Gomez, G.; Norton, S. K.; Zhao, W.; Schwartz, L. B.; Lenk, R.; Kepley, C. L. Fullerene Nanomaterials Inhibit the Allergic Response. *J. Immunol. Baltim. Md 1950* **2007**, *179*, 665–672.
- (14) Li, S.; Zhao, X.; Mo, Y.; Cummings, P. T.; Heller, W. T. Human Serum Albumin Interactions with C60 Fullerene Studied by Spectroscopy, Small-Angle Neutron Scattering, and Molecular Dynamics Simulations. *J. Nanoparticle Res.* **2013**, *15*, 1–11.
- (15) Benyamini, H.; Shulman-Peleg, A.; Wolfson, H. J.; Belgorodsky, B.; Fadeev, L.; Gozin, M. Interaction of c(60)-Fullerene and Carboxyfullerene with Proteins: Docking and Binding Site Alignment. *Bioconjug. Chem.* **2006**, *17*, 378–386.
- (16) Chen, B.-X.; Wilson, S. R.; Das, M.; Coughlin, D. J.; Erlanger, B. F. Antigenicity of Fullerenes: Antibodies Specific for Fullerenes and Their Characteristics. *Proc. Natl. Acad. Sci.* **1998**, *95*, 10809–10813.
- (17) Bosi, S.; Ros, T. D.; Spalluto, G.; Prato, M. Fullerene Derivatives: An Attractive Tool for Biological Applications. *Eur. J. Med. Chem.* **2003**, *38*, 913–923.
- (18) Chen, Z.; Ma, K.; Wang, G.; Zhao, X.; Tang, A. Structures and Stabilities of C60(OH)4 and C60(OH)6 Fullerenols. *J. Mol. Struct. THEOCHEM* **2000**, *498*, 227–232.
- (19) Eropkin, M. Y.; Melenevskaya, E. Y.; Nasonova, K. V.; Bryazzhikova, T. S.; Eropkina, E. M.; Danilenko, D. M.; Kiselev, O. I. Synthesis and Biological Activity of Fullerenols with Various Contents of Hydroxyl Groups. *Pharm. Chem. J.* **2013**, *47*, 87–91.
- (20) Mikawa, M.; Kato, H.; Okumura, M.; Narazaki, M.; Kanazawa, Y.; Miwa, N.; Shinohara, H. Paramagnetic Water-Soluble Metallofullerenes Having the Highest Relaxivity for MRI Contrast Agents. *Bioconjug. Chem.* **2001**, *12*, 510–514.
- (21) Grebowski, J.; Krokosz, A.; Puchala, M. Fullereneol C60(OH)36 Could Associate to Band 3 Protein of Human Erythrocyte Membranes. *Biochim. Biophys. Acta BBA - Biomembr.* **2013**, *1828*, 2007–2014.
- (22) Kokubo, K. Water Soluble Single-Nano Carbon Particles: Fullereneol and Its Derivatives. In *The delivery of nanoparticles*; InTech, 2012; pp. 317–332.
- (23) Ratnikova, T. A.; Govindan, P. N.; Salonen, E.; Ke, P. C. In Vitro Polymerization of Microtubules with a Fullerene Derivative. *ACS Nano* **2011**, *5*, 6306–6314.
- (24) Nedumpully Govindan, P.; Monticelli, L.; Salonen, E. Mechanism of Taq DNA Polymerase Inhibition by Fullerene Derivatives: Insight from Computer Simulations. *J. Phys. Chem. B* **2012**, *116*, 10676–10683.

- (25) Monticelli, L.; Barnoud, J.; Orłowski, A.; Vattulainen, I. Interaction of C70 Fullerene with the Kv1.2 Potassium Channel. *Phys. Chem. Chem. Phys. PCCP* **2012**, *14*, 12526–12533.
- (26) Wu, X.; Yang, S.-T.; Wang, H.; Wang, L.; Hu, W.; Cao, A.; Liu, Y. Influences of the Size and Hydroxyl Number of Fullerenes/fullerenols on Their Interactions with Proteins. *J. Nanosci. Nanotechnol.* **2010**, *10*, 6298–6304.
- (27) Deng, Z. J.; Liang, M.; Monteiro, M.; Toth, I.; Minchin, R. F. Nanoparticle-Induced Unfolding of Fibrinogen Promotes Mac-1 Receptor Activation and Inflammation. *Nat. Nanotechnol.* **2011**, *6*, 39–44.
- (28) Shang, W.; Nuffer, J. H.; Dordick, J. S.; Siegel, R. W. Unfolding of Ribonuclease A on Silica Nanoparticle Surfaces. *Nano Lett.* **2007**, *7*, 1991–1995.
- (29) Wettern, P. D. M. Cell Physiology — Ubiquitin. In *Progress in Botany*; Behnke, P. D. H.-D.; Esser, P. D. D. h c K.; Kubitzki, P. D. K.; Runge, P. D. M.; Ziegler, P. D. D. h c H., Eds.; Progress in Botany/Fortschritte der Botanik; Springer Berlin Heidelberg, 1992; pp. 153–165.
- (30) Hershko, A.; Ciechanover, A. The Ubiquitin System. *Annu. Rev. Biochem.* **1998**, *67*, 425–479.
- (31) Rapaport, D. C. *The Art of Molecular Dynamics Simulation*; Cambridge University Press: Cambridge, UK; New York, NY, 2004.
- (32) Ding, F.; Tsao, D.; Nie, H.; Dokholyan, N. V. Ab Initio Folding of Proteins with All-Atom Discrete Molecular Dynamics. *Structure* **2008**, *16*, 1010–1018.
- (33) Shirvanyants, D.; Ding, F.; Tsao, D.; Ramachandran, S.; Dokholyan, N. V. Discrete Molecular Dynamics: An Efficient And Versatile Simulation Method For Fine Protein Characterization. *J. Phys. Chem. B* **2012**, *116*, 8375–8382.
- (34) Ding, F.; Radic, S.; Chen, R.; Chen, P.; Geitner, N. K.; Brown, J. M.; Ke, P. C. Direct Observation of a Single Nanoparticle–ubiquitin Corona Formation. *Nanoscale* **2013**, *5*, 9162–9169.
- (35) Käkinen, A.; Ding, F.; Chen, P.; Mortimer, M.; Kahru, A.; Ke, P. C. Interaction of Firefly Luciferase and Silver Nanoparticles and Its Impact on Enzyme Activity. *Nanotechnology* **2013**, *24*, 345101.
- (36) Dobson, C. M. Principles of Protein Folding, Misfolding and Aggregation. *Semin. Cell Dev. Biol.* **2004**, *15*, 3–16.
- (37) Gsponer, J.; Vendruscolo, M. Theoretical Approaches to Protein Aggregation. *Protein Pept. Lett.* **2006**, *13*, 287–293.
- (38) Shang, J.; Ratnikova, T. A.; Anttalainen, S.; Salonen, E.; Ke, P. C.; Knap, H. T. Experimental and Simulation Studies of a Real-Time Polymerase Chain Reaction in the Presence of a Fullerene Derivative. *Nanotechnology* **2009**, *20*, 415101.
- (39) Sayes, C. M.; Fortner, J. D.; Guo, W.; Lyon, D.; Boyd, A. M.; Ausman, K. D.; Tao, Y. J.; Sitharaman, B.; Wilson, L. J.; Hughes, J. B.; *et al.* The Differential Cytotoxicity of Water-Soluble Fullerenes. *Nano Lett.* **2004**, *4*, 1881–1887.
- (40) Pinteala, M.; Dascalu, A.; Ungurenasu, C. Binding Fullerenol C60(OH)24 to dsDNA. *Int. J. Nanomedicine* **2009**, *4*, 193–199.
- (41) Qiao, R.; Roberts, A. P.; Mount, A. S.; Klaine, S. J.; Ke, P. C. Translocation of C60 and Its Derivatives Across a Lipid Bilayer. *Nano Lett.* **2007**, *7*, 614–619.
- (42) Piątek, A.; Dawid, A.; Gburski, Z. The Properties of Small Fullerenol Cluster (C60(OH)24)7: Computer Simulation. *Spectrochim. Acta. A. Mol. Biomol. Spectrosc.* **2011**, *79*, 819–823.

- (43) Yang, S.-T.; Wang, H.; Guo, L.; Gao, Y.; Liu, Y.; Cao, A. Interaction of Fullerenol with Lysozyme Investigated by Experimental and Computational Approaches. *Nanotechnology* **2008**, *19*, 395101.
- (44) Ge, C.; Du, J.; Zhao, L.; Wang, L.; Liu, Y.; Li, D.; Yang, Y.; Zhou, R.; Zhao, Y.; Chai, Z.; *et al.* Binding of Blood Proteins to Carbon Nanotubes Reduces Cytotoxicity. *Proc. Natl. Acad. Sci. U. S. A.* **2011**, *108*, 16968–16973.
- (45) Zuo, G.; Huang, Q.; Wei, G.; Zhou, R.; Fang, H. Plugging into Proteins: Poisoning Protein Function by a Hydrophobic Nanoparticle. *ACS Nano* **2010**, *4*, 7508–7514.
- (46) Jagielska, A.; Scheraga, H. A. Influence of Temperature, Friction, and Random Forces on Folding of the B-Domain of Staphylococcal Protein A: All-Atom Molecular Dynamics in Implicit Solvent. *J. Comput. Chem.* **2007**, *28*, 1068–1082.
- (47) Srinivasan, R.; Rose, G. D. A Physical Basis for Protein Secondary Structure. *Proc. Natl. Acad. Sci.* **1999**, *96*, 14258–14263.
- (48) Mesarič, T.; Baweja, L.; Drašler, B.; Drobne, D.; Makovec, D.; Dušak, P.; Dhawan, A.; Sepčić, K. Effects of Surface Curvature and Surface Characteristics of Carbon-Based Nanomaterials on the Adsorption and Activity of Acetylcholinesterase. *Carbon* **2013**, *62*, 222–232.
- (49) Xu, H.; Wang, D.; He, S.; Li, J.; Feng, B.; Ma, P.; Xu, P.; Gao, S.; Zhang, S.; Liu, Q.; *et al.* Graphene-Based Nanoprobes and a Prototype Optical Biosensing Platform. *Biosens. Bioelectron.* **2013**, *50*, 251–255.
- (50) Podila, R.; Vedantam, P.; Ke, P. C.; Brown, J. M.; Rao, A. M. Evidence for Charge-Transfer-Induced Conformational Changes in Carbon Nanostructure–Protein Corona. *J. Phys. Chem. C* **2012**, *116*, 22098–22103.
- (51) Lynch, I.; Dawson, K. A. Protein-Nanoparticle Interactions. *Nanotoday* **2008**, *3*, 40–47.
- (52) Vijay-Kumar, S.; Bugg, C. E.; Cook, W. J. Structure of Ubiquitin Refined at 1.8Å resolution. *J. Mol. Biol.* **1987**, *194*, 531 – 544.
- (53) Morris, G. M.; Goodsell, D. S.; Halliday, R. S.; Huey, R.; Hart, W. E.; Belew, R. K.; Olson, A. J. Automated Docking Using a Lamarckian Genetic Algorithm and an Empirical Binding Free Energy Function. *J. Comput. Chem.* **1998**, *19*, 1639.
- (54) Hess, B.; Kutzner, C.; Spoel, D. van der; Lindahl, E. GROMACS 4: Algorithms for Highly Efficient, Load-Balanced, and Scalable Molecular Simulation. *J Chem Theory Comput* **2008**, *4*, 435.
- (55) Jorgensen, W. L.; Tirado-Rives, J. The OPLS [optimized Potentials for Liquid Simulations] Potential Functions for Proteins, Energy Minimizations for Crystals of Cyclic Peptides and Crambin. *J. Am. Chem. Soc.* **1988**, *110*, 1657–1666.
- (56) Jorgensen, W. L.; Maxwell, D. S.; Rives, J. T. Development and Testing of the OPLS All-Atom Force Field on Conformational Energetics and Properties of Organic Liquids. *J. Am. Chem. Soc.* **1996**, *118*, 11225–11236.
- (57) Jorgensen, W. L.; Chandrasekhar, J.; Madura, J. D.; Impey, R. W.; Klein, M. L. Comparison of Simple Potential Functions for Simulating Liquid Water. *J. Chem. Phys.* **1983**, *79*, 926–935.
- (58) Bussi, G.; Donadio, D.; Parrinello, M. Canonical Sampling through Velocity Rescaling. *J. Chem. Phys.* **2007**, *126*, 014101.
- (59) Berendsen, H. J. C.; Postma, J. P. M.; Gunsteren, W. F. van; DiNola, A.; Haak, J. R. Molecular Dynamics with Coupling to an External Bath. *J. Chem. Phys.* **1984**, *81*, 3684.

- (60) Parrinello, M.; Rahman, A. Polymorphic Transitions in Single Crystals: A New Molecular Dynamics Method. *J. Appl. Phys.* **1981**, *52*, 7182.
- (61) Hess, B.; Bekker, H.; Berendsen, H. J. C.; Fraaije, J. G. E. M. LINCS: A Linear Constraint Solver for Molecular Simulations. *J. Comput. Chem.* **1997**, *18*, 1463.
- (62) Darden, T.; York, D.; Pedersen, L. Particle Mesh Ewald: An N [center-Dot] log(N) Method for Ewald Sums in Large Systems. *J. Chem. Phys.* **1993**, *98*, 10089–10092.
- (63) Essmann, U.; Perera, L.; Berkowitz, M. L.; Darden, T.; Lee, H.; Pedersen, L. G. A Smooth Particle Mesh Ewald Method. *J. Chem. Phys.* **1995**, *103*, 8577–8593.
- (64) *The PyMOL Molecular Graphics System, Version 1.5.0.4 Schrödinger, LLC.*
- (65) Lakowicz, J. R. *Principles of Fluorescence Spectroscopy*; Springer, 2007.
- (66) Gauthier, T. D.; Shane, E. C.; Guerin, W. F.; Seitz, W. R.; Grant, C. L. Fluorescence Quenching Method for Determining Equilibrium Constants for Polycyclic Aromatic Hydrocarbons Binding to Dissolved Humic Materials. *Environ. Sci. Technol.* **1986**, *20*, 1162–1166.

## Figure Captions

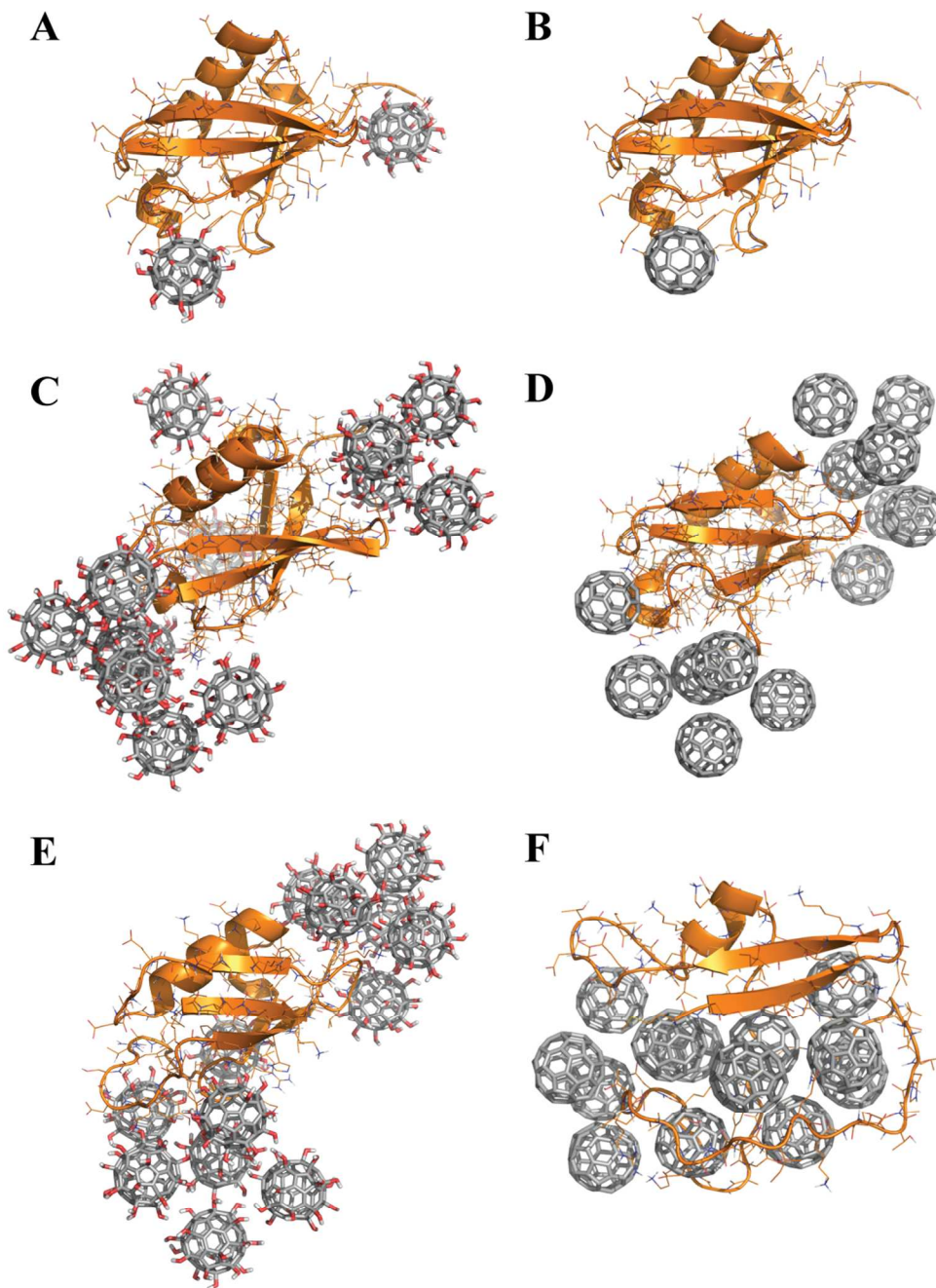


**Figure 1. The predicted binding structures between ubiquitin and fullerene-based nanoparticles.** The computational modeling approaches include molecular docking (A, B), MD simulations with explicit solvent (C, D), and DMD simulations with implicit solvent (E, F). The panels (A, C, E) correspond to the results for fullereneol C<sub>60</sub>(OH)<sub>20</sub> binding, and panels (B, D, F) illustrate the binding with fullerene C<sub>60</sub>. The protein backbone is shown in cartoon and the side-chains are in line representations. The carbon-based nanoparticles are shown in sticks.

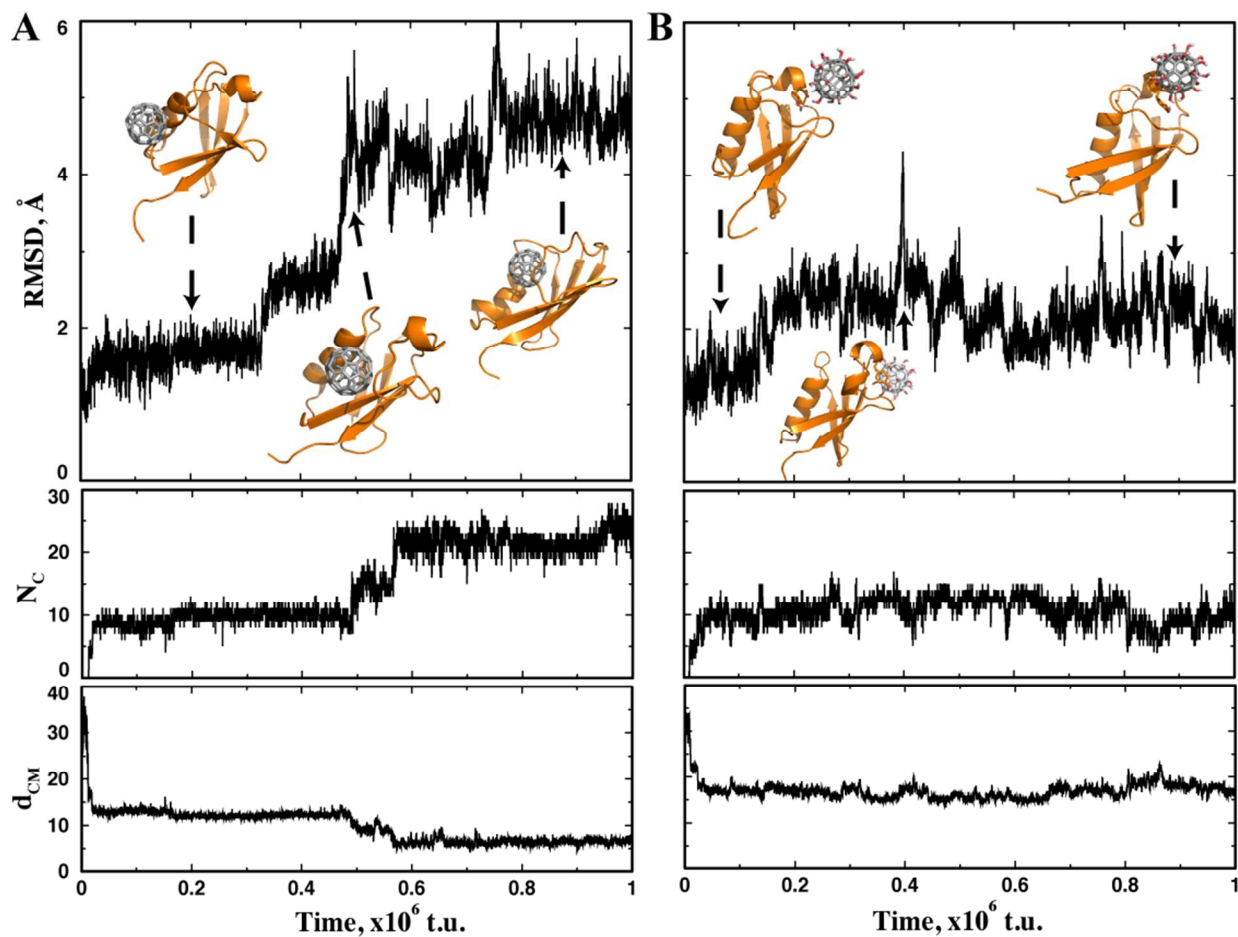


**Figure 2. The binding trajectories in DMD simulations.** Differential conformational dynamics of ubiquitin were observed upon binding fullerene C<sub>60</sub> (A) and fulleranol C<sub>60</sub>(OH)<sub>20</sub> (B). The RMSD of ubiquitin, the number of residues in contact with the nanoparticle ( $N_C$ ), and the intermolecular distance between the corresponding centers of mass ( $d_{CM}$ ) were monitored as the function of simulation time, in the unit of DMD time unit (t.u.; see Methods). The snapshot structures of the protein-nanoparticle complex were shown as inserts along the trajectories.

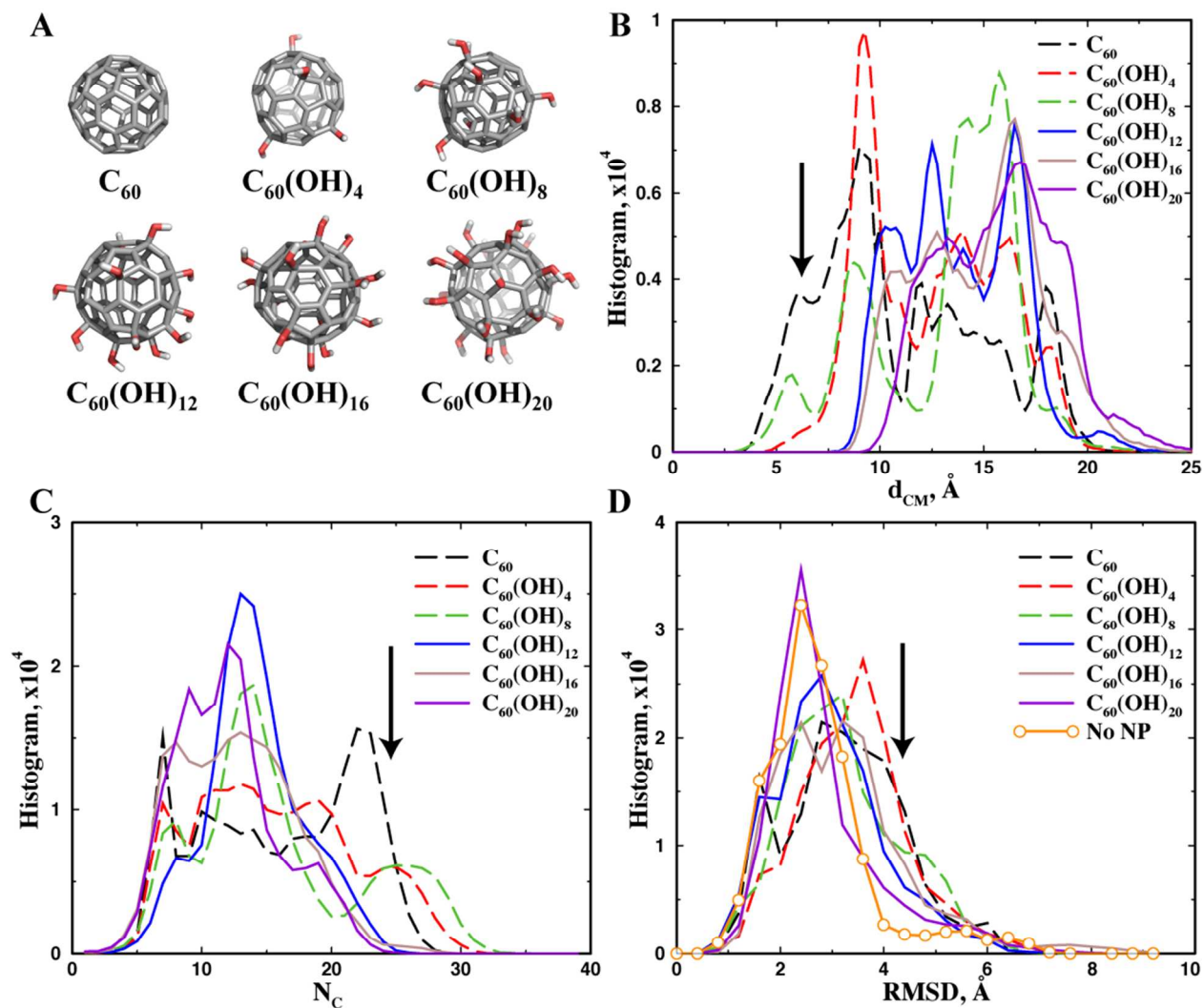


**Figure 3. The equilibrium binding between ubiquitin and fullerenols with various numbers of hydroxyls.** (A) The fullerenols  $C_{60}(OH)_n$  used in simulations, where  $n=0, 4, 8, 12, 16,$  and  $20$ , are shown in sticks. Based on multiple independent DMD simulations with different initial conditions, we computed the histogram of (B) inter-molecular distances,  $d_{CM}$ , (C) number of contacting residues,  $N_C$ , and (D) the RMSD of the protein. The arrows highlight the significant changes in the histogram plots that correlate with the changes in the number of hydroxyl groups.

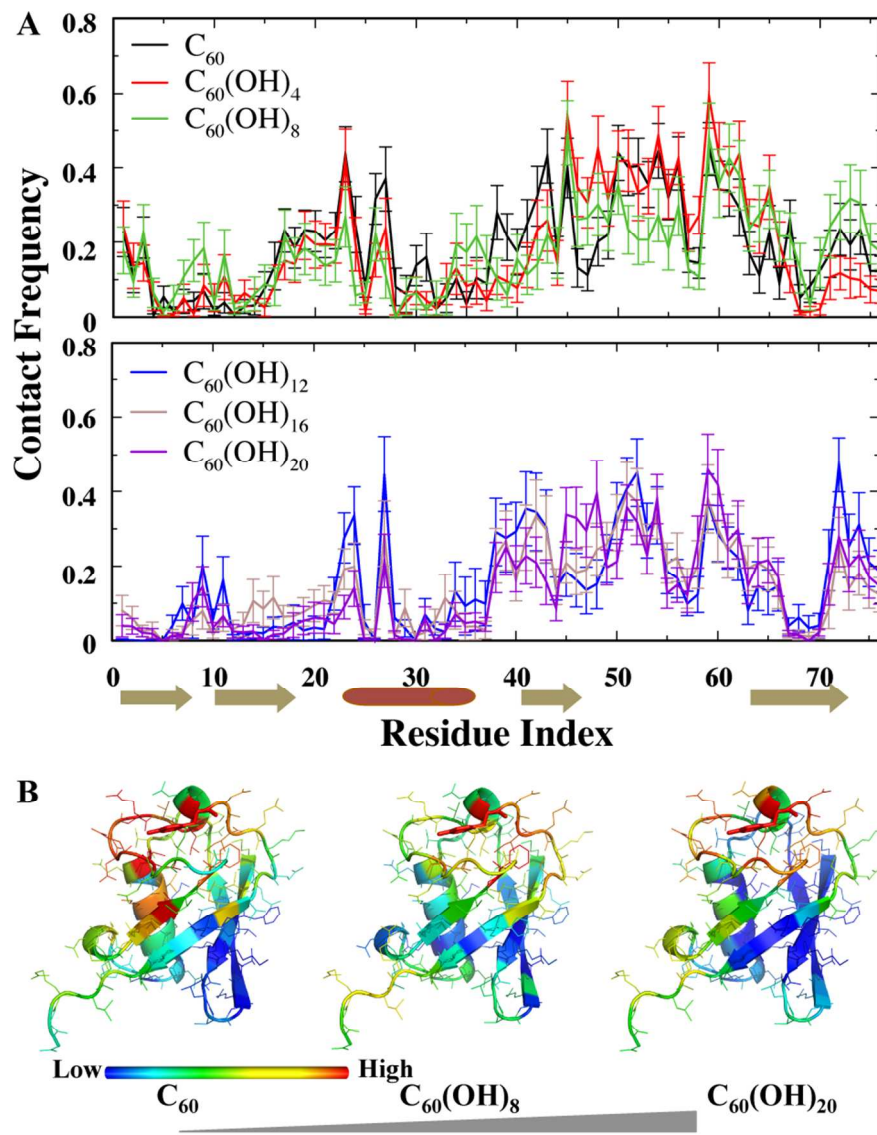


**Figure 4.** The contact frequency between fullerene and each protein residue. (A) The average contact frequency is computed over the independent DMD simulations, and the error bars correspond to the estimated standard errors. The schematics of protein secondary structures were shown underneath the sequence index, where arrows correspond to strands and cylinders denote helices. (B) In the native structure, we colored each residue according to their contact frequencies with respect to the nanoparticle.

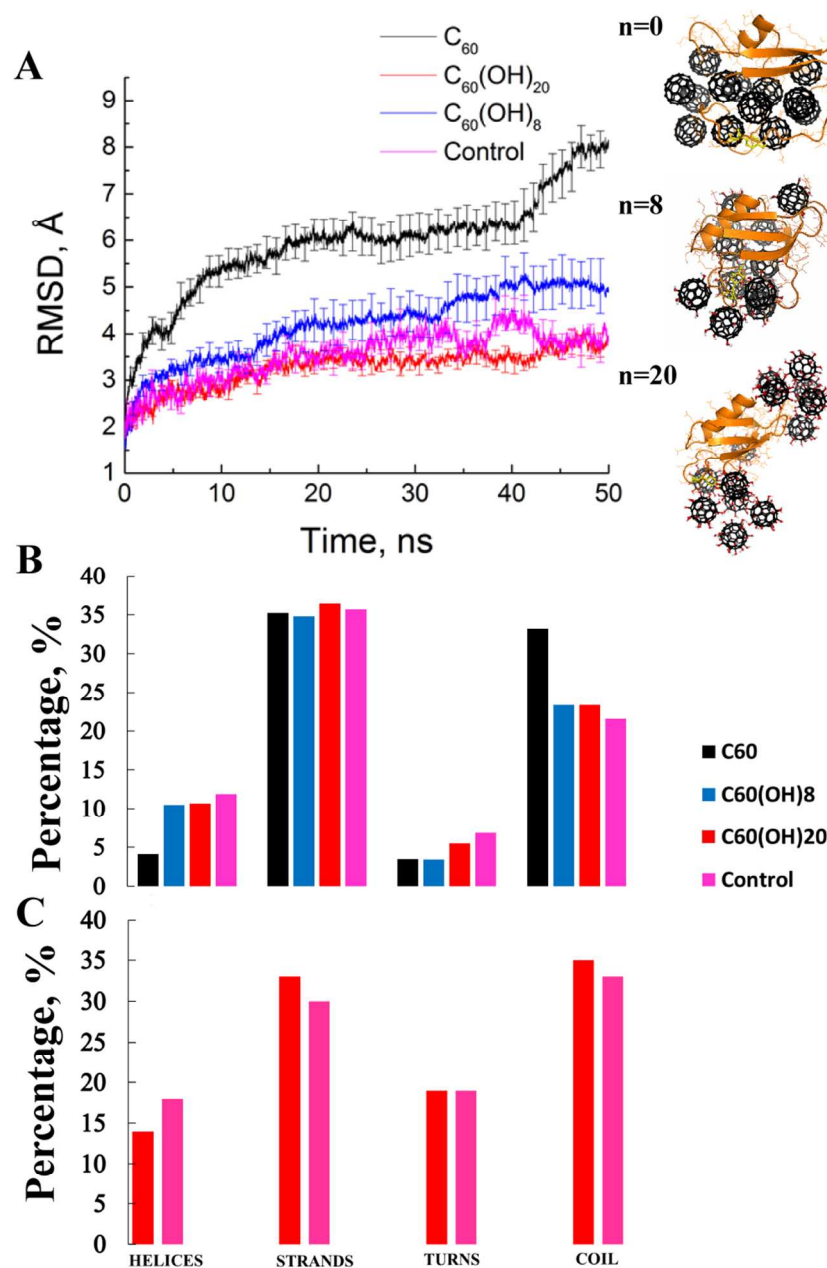


**Figure 5. The tertiary and secondary structures of ubiquitin induced by multiple nanoparticle binding.** (A) We monitored the average RMSD of ubiquitin as the function of DMD simulation time. Typical complex structures obtained from simulations were shown as inserts. The simulations with protein only were used as the control for comparison. (B) The secondary structure contents were computed from DMD simulations of ubiquitin upon binding fullerenols with various numbers of hydroxyls. (C) The experimentally measured protein secondary structure elements.